Research Article | Vol. 26, No. 23 | 12 Nov 2018 | OPTICS EXPRESS 30009
Optics EXPRESS

Patterned illumination single molecule localization microscopy (piSMLM): user defined blinking regions of interest

Shih-Ya Chen,[1] Felix Bestvater,[2] Wladimir Schaufler,[2,3] Rainer Heintzmann,[4,5] and Christoph Cremer[1,3,6,*]

[1]*Institute of Molecular Biology, Mainz 55128, Germany*
[2]*German Cancer Research Center, Im Neuenheimer Feld 280, 69120 Heidelberg, Germany*
[3]*Institute of Pharmacy and Molecular Biotechnology (IPMB), Heidelberg University, 69120, Germany*
[4]*Institute of Physical Chemistry and Abbe Center of Photonics, Friedrich Schiller University Jena, 07743, Germany*
[5]*Leibniz Institute of Photonic Technology, Jena 07745, Germany*
[6]*Physics Department University of Mainz (JGU), Mainz 55128, Germany*
[*]*c.cremer@imb-mainz.de*

Abstract: Single molecule localization microscopy (SMLM) has been established as an important super-resolution technique for studying subcellular structures with a resolution down to a lateral scale of 10 nm. Usually samples are illuminated with a Gaussian shaped beam and consequently insufficient irradiance on the periphery of the illuminated region leads to artifacts in the reconstructed image which degrades image quality. We present a newly developed patterned illumination SMLM (piSMLM) to overcome the problem of uneven illumination by computer-generated holography. By utilizing a phase-only spatial light modulator (SLM) in combination with a modified Gerchberg-Saxton algorithm, a user-defined pattern with homogeneous and nearly speckle-free illumination is obtained. Our experimental results show that irradiance 1 to 5 kW/cm^2 was achieved by using a laser with an output power of 200 mW in a region of 2000 µm^2 to 500 µm^2, respectively. Higher irradiance of up to 20 kW/cm^2 can be reached by simply reducing the size of the region of interest (ROI). To demonstrate the application of the piSMLM, nuclear structures were imaged based on fluctuation binding-activated localization microscopy (fBALM). The super-resolution fBALM images revealed nuclear structures at a nanometer scale.

1. Introduction

Fluorescence microscopy is an important tool for studying a variety of questions in biology. Cellular organelles exhibit very complex molecular structures on different scales, from a few micrometers down to several nanometers. However, fine structures of cell organelles below the optical resolution limit are not observable. The super-resolution method Single Molecule Localization Microscopy (SMLM) was developed to overcome the resolution barrier. The first 'pointillism' method of SMLM was demonstrated by imaging blinking quantum dots (QDs) as light emitters [1]. The QDs signals were distinguished with the help of independent component analysis based on statistical blinking of QDs. This 'pointillism' technique opened avenues to study cellular structure by using photo-switchable fluorophores for biological samples [2–4]. In order to photoactivate or recover fluorophores, such fluorescence microscopes are typically equipped with lasers, which normally have Gaussian irradiance profiles. However, the disadvantage of Gaussian illumination for SMLM is the introduction of uneven illumination in the sample. Depending on the irradiance distribution of the Gaussian illumination, different amounts of fluorescence photons are emitted, which can lead to a higher localization precision in the center region of the Gaussian illumination spot relatively to the outside region [5].

#340954 https://doi.org/10.1364/OE.26.030009
Journal © 2018 Received 16 Aug 2018; revised 5 Oct 2018; accepted 5 Oct 2018; published 31 Oct 2018

Optics EXPRESS

Moreover, molecules in low irradiance areas show a longer on-state, resulting in many overlapping emitters, which introduces artifacts in the reconstructed super-resolution image, thus hampering the quantitative evaluation based on the intensity distribution [6]. Several approaches have been proposed to overcome the inhomogeneity problem over the full field of view. One method to create a flat-top illumination is to insert two micro lens arrays for creating ray bundles. The ray bundles propagate and overlap in the sample plane resulting in a homogenous illumination [7]. Another approach is to use a laser which is coupled into a multimode fiber [8]. The disadvantage of both of these methods is the requirement of fast spatial dithering (e.g. by a rotating diffuser) to eliminate non-uniformities. Some other methods utilize a beam-shaper to convert a Gaussian beam into a flat-top irradiance distribution [9,10]. However, a beam-shaper is commonly designed to generate a circular laser spot, which limits the field of view to a circular illumination area. Additionally, all of the above mentioned methods are limited to a certain shape of illumination and changing the shape requires special design and additional optical components.

To overcome the limitations of current SMLM, we developed a patterned illumination technique for wide-field fluorescence microscopy based on computer-generated holography. By utilizing a phase-only spatial light modulator (SLM) in combination with a Gerchberg-Saxton algorithm (GS) [11], one has the possibility to define arbitrary patterns as regions of interest (ROIs). In order to achieve flat-top illumination with arbitrary desired shapes, we propose a calibration method which can eliminate a slight misalignment or laser induced inhomogeneous illumination by modifying the standard GS algorithm.

In this method, the superposition of a Fresnel lens and the phase mask calculated by our modified GS algorithm separates the pattern from the undesirable zeroth diffraction order, resulting in a high contrast image. Because of the light redistribution in the phase-only SLM, low power losses can be achieved. The advantage of this technique is that the total power in the sample is independent of the size of the illumination pattern. By reducing the ROI, higher irradiance can be achieved. In contrast to our method, placing a modulator in the image plane to define a ROI to achieve patterned illumination by a digital micro-mirror device (DMD) exhibits a linear dependency on the size of the illumination area [12,13]. Therefore, higher illumination irradiance can only be obtained by increasing the laser power. Furthermore, without introducing an additional device to reduce laser speckles in the sample, the time-averaging method was implemented in the software of piSMLM [14–16]. To demonstrate the capability of piSMLM, we first show the influence of non-uniform illumination in wide-field fluorescence microscopy by comparing images of cell nuclei excited by Gaussian illumination with flat-top illumination. Additionally, we show the possibility for user-defined ROIs with high illumination intensities to achieve SMLM super-resolution image.

2. Patterned illumination single molecule localization microscopy setup

2.1 Excitation beam path

A custom-made inverted fluorescence microscope was designed and set up for patterned illumination single molecule localization microscopy. The scheme of the setup is shown in Fig. 1. The microscope was equipped with a 488 nm (Omicron, Germany), a 561 nm (Frankfurt Laser, Germany) and a 647 nm (Cobolt, Sweden) laser with 200 mW, 200 mW and 120 mW of the maximum output power, respectively. The three lasers were combined with dichromatic reflectors D1 and D2. By switching the flip-mirrors M5 and M8, the illumination mode could be chosen between Gaussian illumination and the patterned illumination mode.

Gaussian illumination mode: The laser was expanded by a pair of lenses L1 and L2 (f = 30 mm, f = 60 mm) and focused at the back focal plane of the objective lens (HCX PL APO 100×/NA 1.47 OIL, Leica, Germany) by a tube lens L9 (f = 125 mm). The quadband dichroic mirror D3 (ZT405/488/561/647rpc, Chroma Technology) was used to reflect the laser and to transmit emitted fluorescence light from the sample. In this setup, a Gaussian irradiance

Optics EXPRESS

distribution with a full width at half maximum (FWHM) of 50 µm was created in the focal plane of the objective lens.

Patterned illumination mode: The laser was expanded by a pair of lenses L3 and L4 (f = 10 mm, f = 100 mm) to match the size of the LCoS SLM (Pluto, Holoeye, Germany). The polarization state of the expanded beam was aligned by a lambda half waveplate to match the modulation axis of the liquid crystal layer of the SLM. The phase distribution of the desired intensity pattern was calculated using a modified Gerchberg-Saxton (GS) algorithm.

Elimination of zeroth diffraction order: A typical problem seen in SLM systems is the presence of the zeroth order of unshaped diffracted light reflected by the SLM. This results in a bright spot superimposed on the desired intensity pattern. A common method to separate this zeroth order and the desired intensity pattern is to add the phase function of a blazed phase grating to tilt the diffracted light from on-axis to off-axis [17]. However, the spatial separation of the desired intensity pattern and the zeroth order requires an off axis propagation of the zeroth order through the optical system, which results in a slightly anisotropic pixel pitch. Another disadvantage is the dispersion introduced by the grating structure resulting in different diffraction angles for the aligned lasers. Another approach to separate the zeroth order and the desired intensity pattern is to superimpose a Fresnel lens on the phase function [18]. Using this method, the desired intensity pattern and the diffraction-limited spot of the non-diffracted light can be slightly separated along the optical axis. By placing a blocker at the position of the zeroth order spot, this spot can be filtered out. However, the axial separation of the desired intensity pattern and the zeroth order blocker is relatively small. The blocker can remove a severe amount of the desired intensity pattern as well.

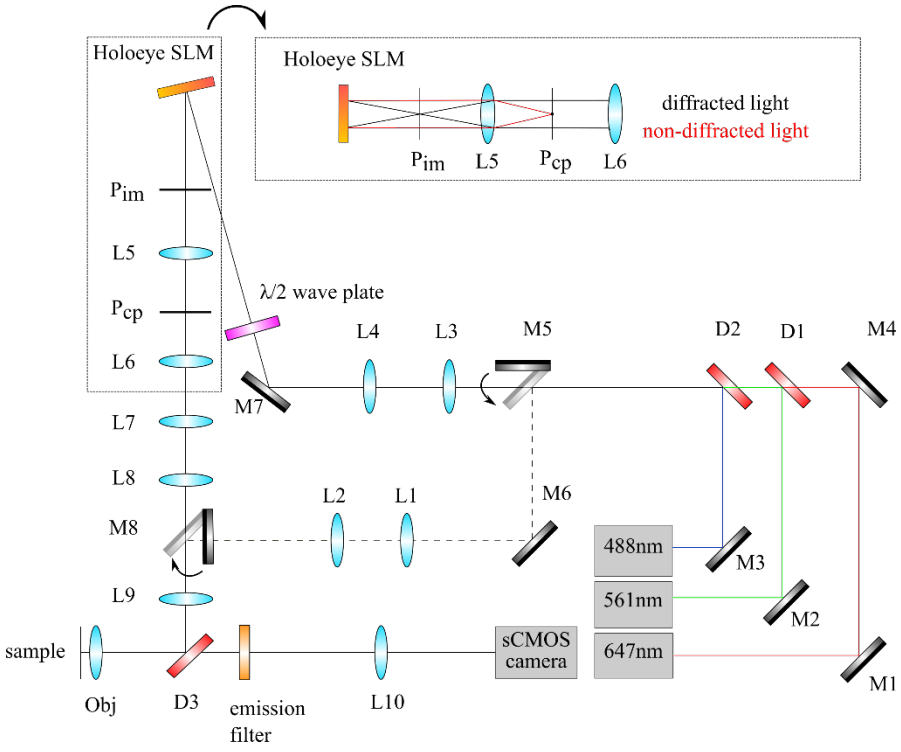

Fig. 1. Patterned illumination single molecule localization microscopy (piSMLM) setup. The inset shows the ray paths of diffracted and non-diffracted light at the SLM, which demonstrates an optimal separation between the desired pattern and the zeroth order originating from the non-diffracted light.

Optics EXPRESS

In our piSMLM setup, we utilized the superposition of the phase distribution calculated by the modified GS algorithm and the phase of a Fresnel lens with a focal length of 110 mm to form an on-axis image at the position P_{im} (see Fig. 1). This image revealed a very uniform background because of the non-diffracted light. Using lens L5, this image was Fourier-transformed into the conjugated pupil plane located at the position P_{cp}. The fine structures of the image were represented by higher frequencies in the conjugated pupil plane. The background due to the non-diffracted light would form a diffraction-limited spot in the center of the conjugated pupil plane. A coverslip with a small central stop was used to filter the non-diffracted light. This high-pass filter had a minimal influence on the higher frequencies of the desired intensity pattern. The filtered low frequencies had minimal impact on the final image. With the lenses L6 (f = 35 mm), L7 (f = 125 mm), L8 (f = 200 mm) and L9 (f = 125 mm) the conjugated pupil plane was relayed to the pupil of the objective lens.

Suppression of laser speckles: Another common problem regarding the GS algorithm is the appearance of speckles. To address this issue, a sequence of phase masks with initial random phases was calculated. Because the initial phase is random, every single desired intensity pattern exhibits a unique speckle pattern. By recording multiple fluorescence images with different speckle patterns and averaging the intensities, an almost speckle-free intensity pattern was obtained [14–16].

Flat-Top Illumination: The almost speckle-free averaged intensity pattern with low speckle noise can still show an inhomogeneous intensity distribution over the entire field of view. Several factors can be the reason for this non-uniformity: aberrations due to slight misalignment in the excitation beam path; the influence of the zeroth order blocker; inhomogeneous illumination of the SLM, i.e. by a Gaussian laser beam or the limitation of the convergent iterative process of the standard GS algorithm. To correct for these effects to obtain a flat-top illumination, a modified GS algorithm is presented in Fig. 2.

The standard GS algorithm was extended by introducing a calibration image which weights the target intensity pattern to correct the non-uniformity. The weighting of the target intensity is achieved by dividing element-wise the target intensity pattern by the normalized calibration image. A detailed description how to measure the calibration image is given in section 3.1. A MATLAB GUI interface (Matlab 2014b, Mathworks) was used to define the desired intensity patterns and the phase patterns were calculated using a GPU accelerated Matlab script.

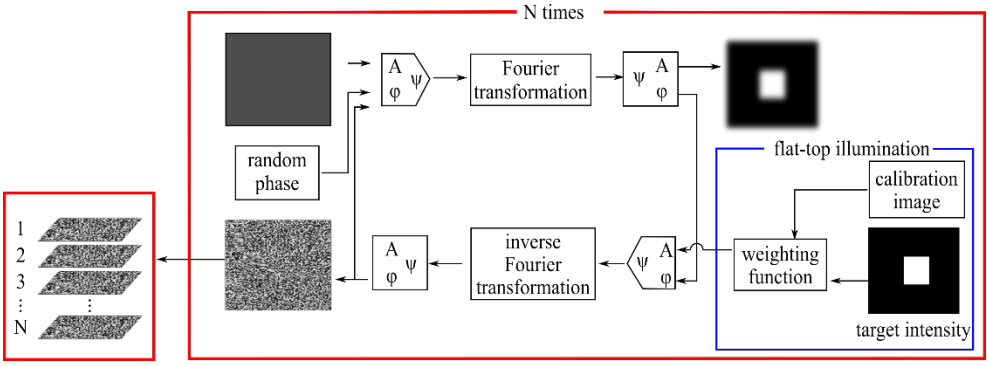

Fig. 2. Flow chart of the modified Gerchberg-Saxton algorithm with wave function ψ, amplitude A and phase φ. The target intensity is weighted by a measured calibration image as a new input intensity to achieve flat-top illumination (blue). Multiple phase masks are generated to remove speckles by the time-averaging method (red).

2.2 Detection beam path

Fluorescence was collected by the objective lens and was separated from the excitation laser by the dichromatic beamsplitter D3. Emission filters (HC609/54, HC520/35, Semrock, ET525/50, ET600/50, ET655, Chroma Technology) were mounted in a motorized filter wheel

Optics EXPRESS

(FW102C, Thorlabs). The emission light was focused by a tube lens (f = 200 mm) and imaged on a sCMOS camera (PCO edge 4.2) with a pixel size corresponding to 65 nm in the sample plane.

3. Experimental results and discussion

3.1 Homogeneously patterned illumination

In the first step, a calibration image for characterizing and correcting the non-uniform illumination was recorded by defining the whole field of view as the desired illumination pattern. Forty corresponding phase masks were calculated using the standard GS algorithm with 20 iterations. After averaging the intensity of the 40 recorded illumination patterns, the image was smoothed with a disk-filter (circular averaging filter) with the size of 30 pixels and normalized to obtain the final calibration image as shown in Fig. 3.

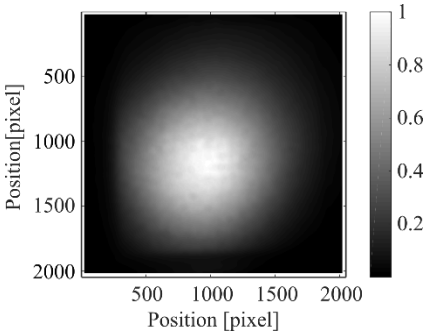

Fig. 3. Calibration image for the full field of view. Pixel size, 65 nm.

To demonstrate the patterned illumination technique, the standard GS algorithm with 20 iterations was used to calculate 40 phase masks of a rectangular ROI with the size of 529 × 492 pixels at the center of the field of view. A mirror sample with nanoholes was used to measure the geometry and the homogeneity of the illumination pattern in the focal plane. By using a LED transmission light source, the position of the mirror was adjusted until the resolution-limited spots of the nanoholes were in the focus. The 488 nm laser was then used to illuminate the sample with the desired pattern. Figure 4(a) shows low speckle noise after averaging 40 images. The intensity profile along the vertical direction of the desired pattern exhibits a pronounced non-uniform profile, as shown in Fig. 4(c) indicated in blue. The same desired pattern was defined to show the improvement of the homogeneous illumination based on the modified GS algorithm (in red). The resulting image is shown in Fig. 4(b).

It can be noted that the region outside of the ROI shows an intensity of less than 5%, because of the limitation of the Gerchberg-Saxton algorithm. The phase retrieval process is fast in the first few iterations, but computing an error-free illumination pattern requires much more iterations due to the slow convergence process [19]. Twenty iterations of the standard or of the modified GS algorithm were chosen to be the optimal number of iterations to achieve a well-defined illumination distribution. The resulting patterned illumination shows a good agreement with the desired pattern as shown in Figs. 4(a) and 4(b).

Optics EXPRESS

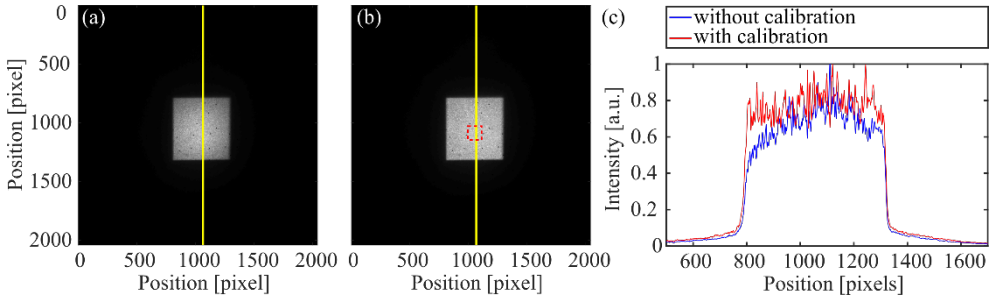

Fig. 4. The averaged intensity of 40 images calculated (a) by the standard GS algorithm and (b) by the modified GS algorithm. The region for the evaluation of the speckle contrast is indicated by the red dashed rectangle. (c) The intensity profiles along the yellow lines are indicated in (a) and (b). Pixel size, 65 nm.

To evaluate the speckles of the resulting image in combination with the modified GS algorithm, the speckle contrast (SC) was used and is defined as [16]:

$$SC = \sigma_s / \langle I \rangle,$$

where σ_s, is the standard deviation of the intensity in the region of the desired pattern, $\langle I \rangle$ is the mean intensity in the same region. We evaluated the speckle contrast in the region of interest indicated as a red dashed rectangle in the desired illumination pattern as shown in Fig. 4(b) by applying 1, 5, 10, 20, 30 and 40 phase masks on the SLM. Our experimental results showed a significant reduction of speckles by displaying multiple phase masks using the time averaging method as shown in Fig. 5. The SC was reduced from 47.59% when only one phase mask was applied to the SLM to 8.09% when 40 images were averaged. Using the time-averaging method, a lower SC can be achieved by displaying a larger number of phase patterns. The SC can be reduced to 3% when 1000 phase masks are displayed on the SLM during image acquisition [16]. Because the SC difference between displaying 30 and 40 phase masks on the SLM is about 1%, 30 phase masks were used in the following experiments to reduce computational time and it was still sufficient for the measurements.

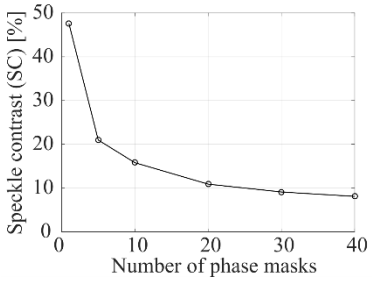

Fig. 5. Experimental results of speckle reduction by the time-averaging method.

To evaluate the influence of Gaussian and flat-top illumination on a biological sample, HeLa cell nuclei were stained with the nucleic acid dye SytoxOrange (Thermo Fisher). The samples were embedded in Dulbecco's Phosphate Buffered Saline (DPBS, Sigma Aldrich) while imaging. A nucleus was chosen and placed in the center of the field of view and excited by the 561 nm laser. The laser was set to low output power to prevent photobleaching, and a band-pass filter ET600/50 (Chroma Technology) was chosen to separate the fluorescence emission of SytoxOrange from the laser beam. Figure 6(a) shows the image of the nucleus under Gaussian illumination. The fluorescent intensity in the center of the nucleus is higher than at the edge. In contrast to the same nucleus illuminated by a flat-top irradiance distribution shown in Fig. 6(b), the image showed much weaker intensity dependence between the center

Optics EXPRESS

and the edge of the nucleus. In each image, the mean value of the background was subtracted as a set-off. Two normalized intensity profiles along two perpendicular axes are shown in Fig. 6(c). The intensity profiles indicate an underestimation of fluorescence signals in the nuclear structure when the nucleus was illuminated by a Gaussian beam. The quantitative evaluation of the intensity differences by using two illumination methods for the same nucleus revealed up to 26% and 25% intensity differences along the long axis and the short axis, respectively. Therefore, it may be essential to illuminate the sample with flat-top illumination in order to ensure a correct intensity-based quantitative evaluation of nuclear structures.

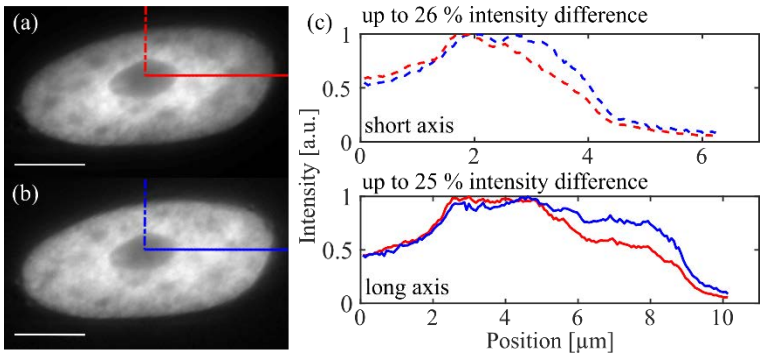

Fig. 6. Imaging of a HeLa cell nucleus by (a) Gaussian illumination and (b) flat-top illumination. (c) The normalized intensity profiles through the cell nucleus in two perpendicular directions (red: Gaussian illumination profiles, blue: flat-top illumination profiles). Scale bar, 5 μm.

The intensity transition is shown between the inside and the outside of the desired illumination region. One half of a nucleus was covered by a ROI indicated by a green rectangle in Figs. 7(a) and 7(b). For a better comparison, the whole nucleus is shown in Fig. 7(a). The mean value of the background in each image was subtracted. Figure 7(c) compares the normalized intensity profiles indicated by a red and a blue line in Figs. 7(a) and 7(b), respectively. A smooth transition of the intensity profile outside of the ROI can be observed. This can be contributed to out-of-focus fluorescence of the cell nucleus due to its extended depth. Furthermore, the low illumination intensity background as discussed in the beginning of this section, leads to a slight additional excitation of fluorophores outside the ROI.

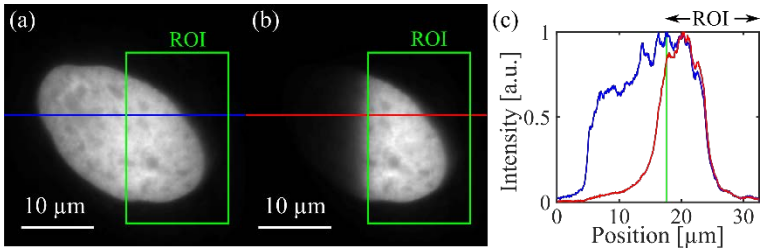

Fig. 7. HeLa cell nucleus images by illuminating (a) the whole cell nucleus and (b) the half of the nucleus. The illumination ROI is indicated by a green rectangle. (c) Normalized fluorescence intensity profiles through the center of the image of (a) and (b) indicated by a blue line (Fig. 7a) and a red line (Fig. 7b), respectively.

3.2 Super-resolution imaging by patterned illumination single molecule localization microscopy (piSMLM)

In the piSMLM setup, arbitrary patterns were generated with a phase-only SLM. In combination with the modified GS algorithm, light was efficiently redistributed. This leads to low power losses because the power was mostly independent of the size of the illumination pattern. The irradiance in the sample was simply increased by decreasing the size of the illumination pattern. This is very advantageous in SMLM applications using appropriate high

Optics EXPRESS

irradiance. In contrast, in the case of a DMD, which acts as an amplitude modulator, the transmitted power depends linearly on the size of the illumination area.

By illuminating the sample with a 561 nm laser, the measured dependency between total laser power in the sample and the size of the ROI was plotted as shown in Fig. 8. The results show that the laser power stays nearly constant for different ROI sizes. Irradiance between 1 and 5 kW/cm^2 could be sufficiently achieved for SMLM experiments at a laser output power of 200 mW. A slight decrease of the laser power in the sample can be seen when a larger ROI was defined. This may be due to a larger contribution of lower frequencies which were removed by the zeroth order blocker.

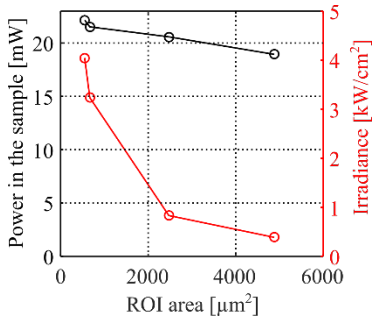

Fig. 8. Plot of laser power versus ROI area and the corresponding irradiance.

We demonstrated the patterned illumination technique for SMLM by imaging cell nuclei based on a recently described super-resolution microscopy method - fluctuation binding-activated localization microscopy (fBALM) [20]. HeLa cell nuclei were stained with DNA intercalator fluorophores - SytoxOrange (Thermo Fisher) and the samples were embedded in Dulbecco's Phosphate Buffered Saline (DPBS, Sigma Aldrich) for wide-field imaging. Two nuclei with elliptical shape were positioned in the center of the field of view and exposed to a low laser power with flat-top illumination to prevent photobleaching. The conventional wide-field image of the two nuclei is shown in Fig. 9(a).

For the fBALM experiment, the buffer was exchanged with the imaging buffer, enzymatic oxygen scavenging, to switch spatially DNA dye molecules between on and off states [20]. The nucleus on the right side was selected to acquire a super-resolution image and the desired target intensity pattern was defined according to the shape of this nucleus. Thirty phase masks were calculated based on the modified GS algorithm. The selected nucleus was exposed to an estimated irradiance of about 1 kW/cm^2 and 20,000 frames were imaged by setting the exposure time to 50 ms. Switching all 30 phase patterns within 50 ms exposure is not possible with the SLM because of the limited frame rate of the device of 60 Hz. Instead, a speckle free reconstructed super-resolution image can be obtained in SMLM, when the 30 phase patterns are sequentially displayed at equal time duration during the whole image acquisition process. Therefore, the 30 calculated phase masks were sequentially displayed on the SLM switching to the next phase mask every 34 s during the image acquisition.

Each illumination pattern shows laser speckles, which leads to a variation of excitation irradiance in the ROI in every single frame. The number of emitted photons may differ resulting in diverse localization precisions, depending on the local illumination irradiance [5]. In case of Gaussian illumination, the localization precision is field-dependent. In contrast, piSMLM exhibits a stochastic distribution of the localization precision in the illuminated area without field dependency. By filtering out the localized molecules with low precision, artifacts in the reconstruction image can be minimized. The stack of images was processed in ThunderSTORM [21]; the reconstructed super-resolution image is shown in Fig. 9(b).

We compared the wide-field image of the two nuclei and the super-resolution image of the nucleus. Since the selected nucleus was under the laser exposure, more than one million blinking dye molecules bound to DNA were localized and the signals were accumulated to

Optics EXPRESS

complete a super-resolution image of the nuclear DNA distribution with an average localization precision of 14.2 nm ± 5.6 nm. Although the left nucleus was not included in the ROI, it was illuminated with a low irradiance as discussed in the section 3.1, sufficient enough to induce a few undesired blinking events due to spatially transient DNA binding mechanism of SytoxOrange based on fBALM [22]. Therefore, a few molecules on the periphery close to the ROI were detected. As shown in Fig. 9(c), the intensity profile of the conventional fluorescence image (Fig. 9(a)) shows relatively smooth SytoxOrange fluorescence transitions in the nucleus, whereas the super-resolution image based on the fBALM method (Fig. 9(b)) reveals high and sharp intensity transitions of the nuclear structure as shown in Fig. 9(d), as expected from the underlying nuclear nanostructure [20,22].

Imaging nuclear structures requires typically at least 20,000 frames to obtain enough DNA molecules for the reconstruction of a super-resolution nuclear image. The total acquisition time is about 1,000 s with a camera exposure time of 50 ms. Hence, it is sufficient to display the calculated 30 phase patterns on the SLM sequentially by switching phase patterns every several seconds. To achieve higher switching frame rates of milliseconds, the synchronization between the SLM and the computer hardware would be necessary. For instance, the speed of the graphics card, which transforms the digital information across the DVI interface to the SLM, the response time of the liquid crystals in the SLM and the implementation of a C++ interface may be optimized. By combining the above mentioned methods, the speed of the switching phase patterns can potentially improve to less than 1 millisecond [23].

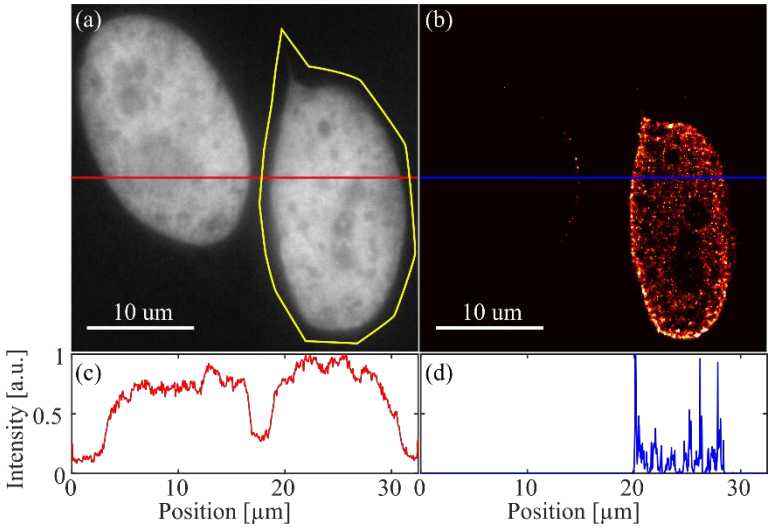

Fig. 9. HeLa cell nuclei images from piSMLM: (a) Conventional wide-field image of two nuclei. The yellow contour line indicates the ROI for light exposure. (b) Super-resolution image of the selected nucleus (right). For a quantitative estimate, the normalized intensity profiles of the conventional wide-field image (c, red) and of the super-resolution fBALM image (d, blue) through the center of the field of view are shown.

3.3 Sample and switching buffer preparation

HeLa cells were cultured in a 25 ml culture flask filled with Dulbecco's Modified Eagle's Medium (DMEM, Thermo Fisher) supplemented with 10% fetal bovine serum (FBS, Thermo Fisher), 1% Penicillin Streptomycin (Pen Strep, Thermo Fisher) and 1% L-Glutamine (Thermo Fisher) in a cell culture incubator (37 °C, 5% CO_2). They were plated at low confluency on a 35 mm chamber (ibidi) and grown overnight. Cells were fixed with pre-warm (37 °C) 4% Formaldehyde (Sigma-Aldrich, 15 min) and washed three times with Dulbecco's Phosphate Buffered Saline (DPBS, Sigma-Aldrich). Afterwards, they were treated with 0.5% Triton X-100 in DPBS (10 min), washed three times with DPBS (5 min) and incubated at 37 °C with

Optics EXPRESS

1:1000 RNase A cocktail (Thermo Fisher) in DPBS overnight. Subsequently, cells were washed with DPBS and nuclei were stained with 0.05 µM SytoxOrange in DPBS (Thermo Fisher; 30 min).

A typical imaging buffer with an enzymatic oxygen scavenging system was prepared for fBALM. The buffer contains 10% glucose (Sigma-Aldrich), 5 mg/ml glucose oxidase from Aspergillus niger (Sigma-Aldrich), 500 µg/ml catalase from bovine liver (Sigma-Aldrich) in DPBS.

4. Conclusion

We demonstrated patterned illumination single molecule localization microscopy (piSMLM) based on computer-generated holography. In contrast to the methods which the illumination is restricted in the field of view [7–10], piSMLM allows users to define arbitrarily shaped illumination regions at any desired position of interest. For example, defining the ROI covering a single cell nucleus allows concentrating all available laser light to the regions of interest instead of spreading it over the entire field of view. Therefore, higher excitation irradiance can be achieved in the ROIs and bleaching of surrounding areas can be avoided. By using the modified GS algorithm in combination with the time-averaging method, problems such as laser speckles and non-uniform illumination were eliminated simply by software implementations without additional optical components. The optical design by superimposing the phase of a Fresnel lens with the SLM phase patterned leads to an excellent separation of the desired patterned and the zeroth diffraction order to form a high contrast illumination area in the focal plane of the objective lens.

We demonstrated our method by imaging cell nuclei to compare flat-top illumination with commonly used Gaussian illumination. When illuminating by a Gaussian laser beam, apparently lower DNA densities on the periphery of the nucleus compared to the center of the nucleus were obtained. In contrast, when exciting with the flat-top illumination, no clear DNA density gradients could be observed. Therefore, it is advantageous to use flat-top illumination for an improved quantitative evaluation of intensity-based images. We demonstrated the potential of the patterned illumination technique with a flat-top irradiance distribution in combination with user-defined ROIs for SMLM. We can achieve high irradiance by defining smaller sizes of ROIs, because of the optical design of the piSMLM setup. As an example, a nucleus was arbitrarily selected and imaged with sufficient irradiance to acquire a super-resolution image with high localization precision.

The patterned illumination technique can be used for many types of microscopes, and it is not restricted to SMLM. For example, the generation of a square flat-top illumination can extend the field of view without edge artifacts for high-throughput microscopy. This microscopy method typically relies on tiling and stitching of multiple fields and the stitched images commonly show distinct dark borders, which degrade the image quality. The patterned illumination technique provides important tools to remove such an artifact without error-prone flat-field correction algorithm [24]. Other applications such as optogenetic applications or fluorescence recovery after photobleaching (FRAP) will also benefit from the freedom of defining single or multiple ROIs arbitrarily for light stimulation [25,26].

Funding

International PhD Programme on Gene Regulation, Epigenetics & Genome Stability, Mainz, Germany; TRR 166 Receptor Light, TP A04; the Leibniz science campus Infecto-Optics, project HotAim.

Acknowledgement

The authors thank Prof. Huang-Ming Chen and Prof. Cheng-Huan Chen (National Chiao Tung University, Taiwan) for discussions about the SLM device; the German Cancer Research

Optics EXPRESS

Center for providing the SLM device as a loan; and Dr. Xiaomin Liu, Dr. Márton Gelléri, Dr. Sandra Ritz, Dr. Mária Hanulová and David Ho for proof reading the manuscript.

References

1. K. Lidke, B. Rieger, T. Jovin, and R. Heintzmann, "Superresolution by localization of quantum dots using blinking statistics," Opt. Express **13**(18), 7052–7062 (2005).
2. E. Betzig, G. H. Patterson, R. Sougrat, O. W. Lindwasser, S. Olenych, J. S. Bonifacino, M. W. Davidson, J. Lippincott-Schwartz, and H. F. Hess, "Imaging intracellular fluorescent proteins at nanometer resolution," Science **313**(5793), 1642–1645 (2006).
3. M. J. Rust, M. Bates, and X. Zhuang, "Stochastic optical reconstruction microscopy (STORM) provides sub-diffraction-limit image resolution," Nat. Methods **3**(10), 793–795 (2006).
4. P. Lemmer, M. Gunkel, D. Baddeley, R. Kaufmann, A. Urich, Y. Weiland, J. Reymann, P. Müller, M. Hausmann, and C. Cremer, "SPDM: light microscopy with single-molecule resolution at the nanoscale," Appl. Phys. B **93**(1), 1–12 (2008).
5. R. E. Thompson, D. R. Larson, and W. W. Webb, "Precise nanometer localization analysis for individual fluorescent probes," Biophys. J. **82**(5), 2775–2783 (2002).
6. A. Burgert, S. Letschert, S. Doose, and M. Sauer, "Artifacts in single-molecule localization microscopy," Histochem. Cell Biol. **144**(2), 123–131 (2015).
7. K. M. Douglass, C. Sieben, A. Archetti, A. Lambert, and S. Manley, "Super-resolution imaging of multiple cells by optimised flat-field epi-illumination," Nat. Photonics **10**(11), 705–708 (2016).
8. J. Deschamps, A. Rowald, and J. Ries, "Efficient homogeneous illumination and optical sectioning for quantitative single-molecule localization microscopy," Opt. Express **24**(24), 28080–28090 (2016).
9. I. Khaw, B. Croop, J. Tang, A. Möhl, U. Fuchs, and K. Y. Han, "Flat-field illumination for quantitative fluorescence imaging," Opt. Express **26**(12), 15276–15288 (2018).
10. C. J. Rowlands, F. Ströhl, P. P. V. Ramirez, K. M. Scherer, and C. F. Kaminski, "Flat-field super-resolution localization microscopy with a low-cost refractive beam-shaping element," Sci. Rep. **8**(1), 5630 (2018).
11. R. W. Gerchberg and W. O. Saxton, "A practical algorithm for the determination of phase from image and diffraction plane pictures," Optik (Stuttg.) **35**(2), 237–246 (1972).
12. L. Valiya Peedikakkal, V. Steventon, A. Furley, and A. J. Cadby, "Development of targeted STORM for super resolution imaging of biological samples using digital micro-mirror device," Opt. Commun. **404**, 18–22 (2017).
13. V. Nikolenko, D. S. Peterka, R. Araya, A. Woodruff, and R. Yuste, "Spatial light modulator microscopy," Cold Spring Harb. Protoc. **2013**(12), 1132–1141 (2013).
14. Y. Takaki and M. Yokouchi, "Speckle-free and grayscale hologram reconstruction using time-multiplexing technique," Opt. Express **19**(8), 7567–7579 (2011).
15. W.-F. Hsu and C.-F. Yeh, "Speckle suppression in holographic projection displays using temporal integration of speckle images from diffractive optical elements," Appl. Opt. **50**(34), H50–H55 (2011).
16. J. W. Goodman, "Some fundamental properties of speckle," J. Opt. Soc. Am. **66**(11), 1145–1150 (1976).
17. A. Jesacher, S. Bernet, and M. Ritsch-Marte, "Broadband suppression of the zero diffraction order of an SLM using its extended phase modulation range," Opt. Express **22**(14), 17590–17599 (2014).
18. P. Pozzi, D. Gandolfi, M. Tognolina, G. Chirico, J. Mapelli, and E. D'Angelo, "High-throughput spatial light modulation two-photon microscopy for fast functional imaging," Neurophotonics **2**(1), 015005 (2015).
19. J. R. Fienup, "Phase retrieval algorithms: a comparison," Appl. Opt. **21**(15), 2758–2769 (1982).
20. A. Szczurek, L. Klewes, J. Xing, A. Gourram, U. Birk, H. Knecht, J. W. Dobrucki, S. Mai, and C. Cremer, "Imaging chromatin nanostructure with binding-activated localization microscopy based on DNA structure fluctuations," Nucleic Acids Res. **45**(8), e56 (2017).
21. M. Ovesný, P. Křížek, J. Borkovec, Z. Švindrych, and G. M. Hagen, "ThunderSTORM: a comprehensive ImageJ plug-in for PALM and STORM data analysis and super-resolution imaging," Bioinformatics **30**(16), 2389–2390 (2014).
22. A. Szczurek, U. Birk, H. Knecht, J. Dobrucki, S. Mai, and C. Cremer, "Super-resolution binding activated localization microscopy through reversible change of DNA conformation," Nucleus **9**(1), 182–189 (2018).
23. R. Förster, H.-W. Lu-Walther, A. Jost, M. Kielhorn, K. Wicker, and R. Heintzmann, "Simple structured illumination microscope setup with high acquisition speed by using a spatial light modulator," Opt. Express **22**(17), 20663–20677 (2014).
24. J. Chalfoun, M. Majurski, T. Blattner, K. Bhadriraju, W. Keyrouz, P. Bajcsy, and M. Brady, "MIST: Accurate and Scalable Microscopy Image Stitching Tool with Stage Modeling and Error Minimization," Sci. Rep. **7**(1), 4988 (2017).
25. L. Valon, A. Marín-Llauradó, T. Wyatt, G. Charras, and X. Trepat, "Optogenetic control of cellular forces and mechanotransduction," Nat. Commun. **8**, 14396 (2017).
26. C. Nakada, K. Ritchie, Y. Oba, M. Nakamura, Y. Hotta, R. Iino, R. S. Kasai, K. Yamaguchi, T. Fujiwara, and A. Kusumi, "Accumulation of anchored proteins forms membrane diffusion barriers during neuronal polarization," Nat. Cell Biol. **5**(7), 626–632 (2003).

Optics EXPRESS